CrossMark

Flame Acceleration in SN Ia Induced by the Burning of Local Unreacted Islands

Tao Shu[1], Yang Gao[2], and Chung K. Law[3]
[1] Center for Combustion Energy and Department of Thermal Engineering, Tsinghua University, Beijing 100084, People's Republic of China
[2] School of Physics and Astronomy, Sun Yat-Sen University, Zhuhai, Guangdong 519082, People's Republic of China; gaoyang25@mail.sysu.edu.cn
[3] Department of Mechanical and Aerospace Engineering, Princeton University, Princeton, NJ 08544, USA

Abstract

The mechanism of type Ia supernova explosions is still unsolved due to the uncertainties in the processes of flame acceleration and the associated deflagration to detonation transition. In carbon–oxygen (C–O) white dwarfs, due to the well known Rayleigh–Taylor (R-T) instability and turbulent vortices in the R-T fingers, there exist unburned islands embedded in the downstream of the main flame front. The burning of such islands can be modeled by the spherical inward-propagating two-step C–O flame, which will accelerate while propagating inward due to the stretch effect and the Zel'Dovich mechanism. In turbulent flows under proper conditions, such acceleration can be further strengthened by turbulent mixing, possibly making the burning of these islands speed up to be supersonic. The supersonic burning of the embedded islands is then a source of heating that speeds up the main flame. Here we derive the relationship between the flame's spontaneous inward-propagating speed and the flame radius in consuming the unburned islands based on the Zel'Dovich mechanism in both laminar and turbulent flows. The calculation results show that, in suitable turbulent situation, i.e., for a C–O white dwarf with density $3.5 \times 10^7\,\mathrm{g\,cm^{-3}}$, Reynolds number 1.0×10^{13}, and integral scale 110 km, the island flame speed reaches the sound speed when the flame radius is 1.5 times the flame thickness, and then remains supersonic. Such supersonic combustion generates shock waves, which heat and speed up the main flame, and possibly lead to the initiation of global detonation.

Unified Astronomy Thesaurus concepts: Hydrodynamics (1963); Shocks (2086); Type Ia supernovae (1728); Astrophysical explosive burning (100)

1. Introduction

SN Ia is a member of the supernova (SN) family, originating from nuclear burning and explosion of a carbon–oxygen (C–O) white dwarf with a mass close to the Chandrasekhar mass. Although its observation serves as one of the most important methods for measuring astronomical distances, the dynamics of nuclear flame burning and how this leads to explosions producing different SN light curves are still unknown (Höflich et al. 1995; Hillebrandt & Niemeyer 2000). Efforts to solve the SN Ia explosion problem in the last two decades have mainly focused on the flame self-acceleration and the subsequent deflagration to detonation transition (DDT; Khokhlov et al. 1997; Gamezo et al. 2002; Röpke 2007; Pan et al. 2008; Schmidt et al. 2010; Woosley et al. 2009, 2011; Malone et al. 2014). However, the mechanism of detonation ignition still remains unidentified because of insufficient study of the flame thickness.

Considering microscopic mechanisms on the scale of the flame thickness, both flame stretch and a decreasing reaction gradient can lead to flame acceleration (Zel'Dovich 1980; Chen et al. 2010). Zel'Dovich et al. (1970) and Zel'Dovich (1980) identified the detonation mechanism through the reaction gradient, i.e., when the temperature gradient of the unburned mixture is small and close to homogeneous, it induces a decreasing reaction gradient. In the most extreme situation of a vanishing temperature gradient, the entire unburned mixture starts to react almost simultaneously, leading to very high flame propagation speeds that exceed the usual flame speed. When it reaches the sound speed, the pressure wave couples with the reaction wave, they strengthen each other, and this eventually develops into a detonation.

In the C–O white dwarf flame, there are situations in which a declining reaction gradient can occur, which could possibly induce the nuclear reaction to transform it into a detonation. Here we look into the burning of an unburned island ignited from its outer boundary. As background, Rayleigh–Taylor (R-T) instability forms unburned islands where a two-step C–O flame can initiate from the boundary and propagate inward, with the following structure: carbon reacts first because of the lower activation energy, and then the oxygen reaction is initiated after a delay (Woosley et al. 2011). Because of the stretch effect, the carbon flame accelerates.[4] Finally the following oxygen flame is accelerated by both the speedup of the carbon flame and the additional reduction of the oxygen reaction gradient caused by the increase of the flame temperature.

If we additionally consider turbulent combustion, there exist unburned islands formed by turbulent vortices as well. These vortices have a wide range of length scales, with the largest vortex reaching the integral scale, which can be as large as $\sim$100 km (Woosley et al. 2009). The scale of the smallest vortex is determined by both the integral scale l_0 and the Reynolds number Re, which is proportional to $l_0 Re^{-3/4}$. For a strong turbulent flow, the sizes of the smallest vortices are possibly between the thickness of the flame and the reaction zone (Pope 2000). These vortices then penetrate into the

---

[4] The stretch effect describes a flame whose surface has positive/negative curvature and the flame stretch reduces/increases the flame temperature, thus slowing down/speeding up the flame when the Lewis number is larger than one, or the opposite when the Lewis number is smaller than one (Taylor 1950; Law 1989; Williams 2000; Chen et al. 2010). For an inward-propagating flame, the curvature is negative, and the Lewis number of carbon burning is much larger than one ($\sim 10^5$), thus the carbon flame temperature and flame speed increase due to the flame stretch effect.
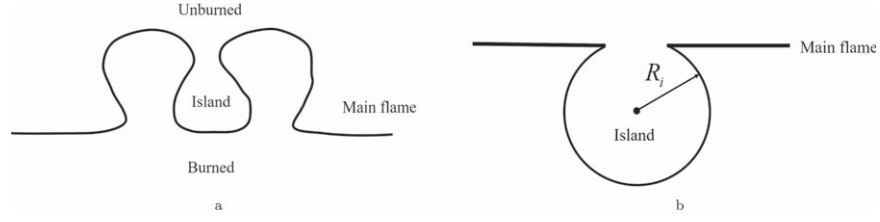
Figure 1. (a) Wrinkled flame forms unburned island; (b) assumption the island is a sphere.

preheat zone of the flame without destroying the flame structure, and have an obvious effect on flame acceleration because they strengthen the mass and thermal diffusion in the broadened preheat zone (Zimont 1979; Kim & Menon 2000; de Goey et al. 2005). As they maintain the laminar flame structure, the turbulent flames under such conditions should also experience additional acceleration due to the stretch effect and the reduced reaction gradient discussed above, thus they are more likely to propagate supersonically.

As a consequence, this paper focuses on how two-step C–O combustion promotes the development of local detonation in the inward burning of the unburned islands formed by the R-T instability and turbulent vortices. We first illustrate the structure of unburned islands in the downstream of the main flame front in Section 2. For the burning of these islands, we apply the Zel'Dovich mechanism in the spherical inward-propagating two-step C–O flames in both laminar and turbulent flows in Sections 3 and 4, respectively. In Section 5 we discuss how such local microdetonations heat and speed up the main flame, possibly leading to global detonation.

2. Spherical Inward-burning Islands Formed by R-T Instability

Due to the R-T instability, the flame surface of SN Ia wrinkles and forms a series of unburned islands embedded within the main flame, as schematically shown in Figure 1(a). The scale of the islands is around the order $\sim$100 cm, allowing variation of a few orders in the typical conditions for SN Ia flame as provided by the simulation of Bell et al. (2004). In turbulent flames there are vortices from the largest to the smallest scales, where the moderate vortices can also form local unburned islands. Such islands are also expected to form frequently in turbulent flows, as will be discussed in Section 5. To simplify the problem, we treat the island as a sphere tangential to the main flame surface, as shown in Figure 1(b). In real flames, the shape of the islands is irregular. However, as the flame curvature is always negative in the burning of the islands, the flame acceleration due to the stretch effect discussed below always applies mechanistically. Variations from the spherical assumption made here can be considered in numerical simulations at the flame structure level.

Inside the island is the unburned mixture of carbon and oxygen, and outside the island is the hot product of the C–O flame. The ignition temperature of the carbon–carbon (C–C) nuclear reaction is lower than that of the oxygen–oxygen (O–O) reaction, so the C–C reaction starts from the boundary of the unburned islands, and the heat released from the C–C reaction ignites the O–O reaction, forming the spherical inward-propagating two-step flame where the carbon flame leads the oxygen flame. The structure of the flame temperature and components' fractions are schematically shown in Figure 2. In the next two sections, we discuss the inward propagation of this
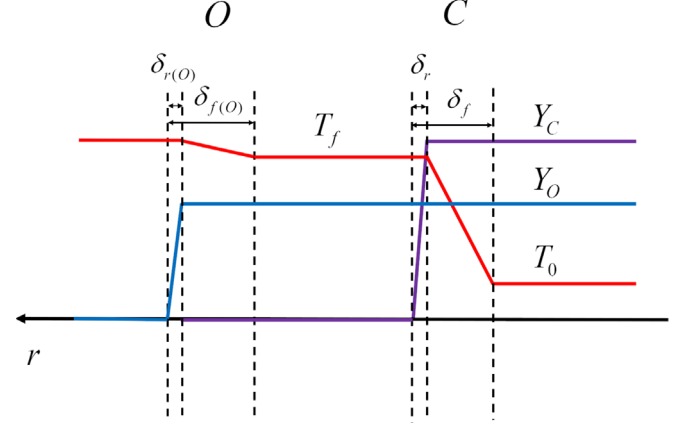

Figure 2. Schematic diagram of a two-step C–O flame with r being the flame radius; the red line is temperature, and the purple and blue lines are mass fractions of carbon and oxygen, respectively. For the inward-propagating island flame considered here, the right is the unburned mixture inside the flame front, and the left is the burned ashes outside of it. $\delta_{f(O)}$ and $\delta_{r(O)}$ are the flame thickness and reaction zone thickness of the oxygen flame. δ_f and δ_r represent the same parameters of the carbon flame. We omit the subscript "C" in the carbon flame thickness and reaction zone thickness, as they will be frequently used hereafter.
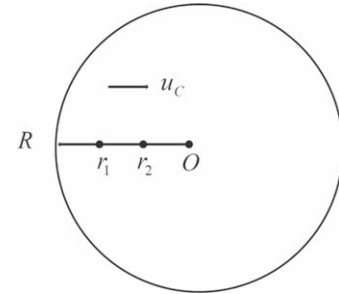

Figure 3. Spherical inward-propagating flame describing the burning of an unburned island.

two-step C–O spherical flame in both laminar and turbulent flows.

3. Spherical Inward-propagating Flame in a Laminar Flow

Zel'Dovich (1980) proposed the concept of spontaneous flame speed from the perspective of the variation of the ignition delay time. For a combustible mixture, when the gradient of the reaction is very small, the time interval of the reaction ignition between two adjacent points is short, which will induce a very high spontaneous propagation flame speed, and may develop into a detonation. Here we look into the reaction gradient of the oxygen burning caused by the leading carbon flame.

As shown in Figure 3, for a spherical inward-propagating flame, the flame starts from the boundary R, and passes r_1 first, with the propagation distance being $R - r_1$; it then passes r_2,

with the propagation distance being $R - r_2$. The instantaneous propagation speed of the oxygen flame can be written as

$$u_{\rm sp(O)} = \frac{(R - r_2) - (R - r_1)}{t_2 - t_1} = \frac{r_1 - r_2}{t_2 - t_1}, \qquad (1)$$

where t_1 and t_2 indicate the time when oxygen begins to burn at the position r_1 and r_2 respectively. Since the oxygen flame follows the carbon flame, the time at which oxygen begins to burn is the carbon flame propagating time plus the oxygen ignition delay time at that point. Due to the stretch effect in the spherical flame, the carbon flame temperature varies with the flame radius, and accordingly the carbon flame speed and oxygen ignition delay time vary and can be expressed as functions of the carbon flame radius.

The time that the carbon flame propagates from R to r can be expressed as $t = \int_R^r \frac{-dr}{u_C(r)}$, with $u_C(r)$ being the carbon flame speed at radius r. If we note the oxygen ignition delay times at the points r_1 and r_2 as $\tau(r_1)$ and $\tau(r_2)$ respectively, the moments of the oxygen flame ignition at the points r_1 and r_2 are

$$t_1 = \int_R^{r_1} \frac{-dr}{u_C(r)} + \tau(r_1), \qquad (2)$$

$$t_2 = \int_R^{r_2} \frac{-dr}{u_C(r)} + \tau(r_2). \qquad (3)$$

Taking the above equations into Equation (1), setting $r_2 = r$, $r_1 = r + dr$, and letting dr tend to zero, we obtain the expression of the spontaneous oxygen flame speed in the one-dimensional two-step C–O flame:

$$u_{\rm sp(O)} = \frac{1}{1/u_C(r) - d\tau(r)/dr}. \qquad (4)$$

It can be seen from the above formula that the spontaneous oxygen flame speed $u_{\rm sp(O)}$ is closely related to both the carbon flame speed $u_C(r)$ and the oxygen ignition delay time $\tau(r)$. Then, to determine $u_{\rm sp(O)}$, we study the relationship between $u_C(r)$, $\tau(r)$ and the flame radius r in the following two subsections, respectively.

3.1. The Carbon Flame Speed at Different Radii

For a one-dimensional spherical flame, the energy equation and component equation of the C–C nuclear reaction in the spherical coordinate can be written as

$$\rho C_p \frac{\partial \tilde{T}}{\partial \tilde{t}} = \frac{1}{\tilde{r}^2} \frac{\partial}{\partial \tilde{r}} \left(\tilde{r}^2 \lambda \frac{\partial \tilde{T}}{\partial \tilde{r}} \right) + q_C \tilde{\omega}_C, \qquad (5)$$

$$\rho \frac{\partial \tilde{Y}}{\partial \tilde{t}} = \frac{1}{\tilde{r}^2} \frac{\partial}{\partial \tilde{r}} \left(\tilde{r}^2 \rho D \frac{\partial \tilde{Y}}{\partial \tilde{r}} \right) - \tilde{\omega}_C, \qquad (6)$$

where the parameters ρ, C_p, λ, q_C, D are density, specific heat, heat transfer coefficient, C–C reaction energy release, and mass transfer coefficient; and the variables $\tilde{T}$, $\tilde{Y}$, $\tilde{\omega}_C$, $\tilde{r}$, and $\tilde{t}$ are the temperature, carbon mass fraction, C–C reaction rate, radius, and time, respectively. Chen et al. (2010) showed that the dimensionless flame temperature and flame speed have the following relation with the flame radius, which we adopt for the

C–C flame:

$$T_f = \frac{1}{u_C(r) - \frac{2}{r}} \omega_C, \qquad (7)$$

$$\left(u_C - \frac{2}{r} \right) \ln \left[\left(u_C - \frac{2}{r} \right)^2 \right] = (Ze - 2) \frac{2}{r} \left(\frac{1}{Le} - 1 \right), \qquad (8)$$

with the following nondimensionalization:

$$u_C = \frac{\tilde{u}}{u_l}, \ r = \frac{\tilde{r}}{\delta_f}, \ T = \frac{\tilde{T} - T_u}{T_b - T_u}, \ t = \frac{\tilde{t}}{\delta_f/u_l}, \ \omega_C = \frac{\tilde{\omega}_C}{\rho u_l/\delta_f}, \qquad (9)$$

where the dimensionless variable u_C is the carbon spherical flame speed, u_l is the carbon laminar flame speed, $T_b = T_u + Y_C q_C/C_p$ is the adiabatic C–C flame temperature, T_u is the unburned temperature and δ_f the C–C laminar flame thickness is as shown in Figure 2. Here the Zel'dovich number $Ze = \frac{T_b - T_u}{3T_b} \sqrt[3]{\frac{E_a}{T_b}}$ and Lewis number $Le = \frac{\lambda}{\rho C_p D}$ are treated as constants in the flame.

Based on the above equations of the carbon flame temperature (7), and flame speed (8) relative to the flame radius, we can obtain their numerical solutions. For the C–O white dwarf with density $3.5 \times 10^7 \, {\rm g \, cm^{-3}}$, we have $Ze = 19.0$, $Le = 10^5$, and the C–C planar flame temperature is $3.7 \times 10^9 \, {\rm K}$ (Woosley et al. 2009). Under this typical condition, the carbon flame temperature and speed increase while the flame propagates inwardly, as shown in Figure 4(a) and (b). When the carbon flame propagates to the radius of one flame thickness, the flame speed increases to 9.8 times the planar flame speed.

3.2. The Oxygen Ignition Delay Time at Different Radii

Here, we derive the relationship between the oxygen ignition delay time and the flame position. The oxygen ignition delay time, defined by the time needed for the oxygen to be consumed to a certain portion, e.g., 95%, of its initial value (Williams 1985), depends on the preheat temperature. In the two-step flame considered here, the oxygen preheat temperature can be approximated to the carbon flame temperature T_f, which increases as the flame propagates inward (7).

As a function of the preheat temperature, the O–O reaction rate can be written as the product of the density and mass fraction changing rate, i.e.,

$$\omega_O(Y_O, T_f) = \rho \frac{dY_O}{dt}. \qquad (10)$$

Integrating (10) from the initial moment to the end of the oxygen ignition, we can get

$$\int_0^{\tau} dt = \int_{Y_{t=0}}^{Y_{t=\tau}} \frac{\rho dY_O}{\omega_O(Y_O, T_f)}. \qquad (11)$$

The left side of the above equation is the oxygen ignition delay time; on the right side, the relative oxygen mass fraction varies from $Y_{t=0} = 1$ the initial value to $Y_{t=\tau} = 1 - \Delta Y$ at the end of the ignition with $\Delta Y = 5\%$, i.e.,

$$\tau = \int_1^{1-\Delta Y} \frac{\rho dY_O}{\omega_O(Y_O, T_f)}. \qquad (12)$$
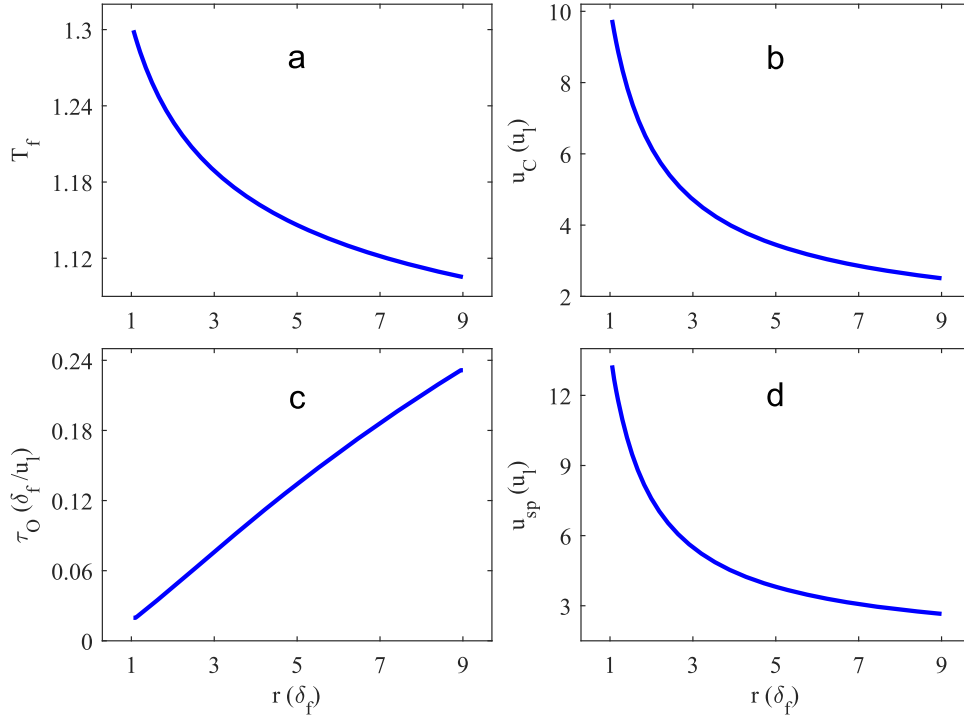
Figure 4. The carbon flame temperature, carbon flame speed, oxygen ignition delay time and oxygen spontaneous propagation flame speed as functions of the flame position. The results shown here are for the C–O white dwarf with $\rho = 3.5 \times 10^7$ g cm^{-3}, $Ze = 19.0$, $Le = 10^5$, and the C–C planar flame temperature being 3.7×10^9 K (Woosley et al. 2009). (a) With the flame propagating inward, the carbon flame temperature goes up because of the stretch effect; (b) the carbon flame accelerates due to the increasing flame temperature; (c) the oxygen ignition delay time decreases due to the increasing carbon flame temperature; (d) the spontaneous oxygen flame speed increases under the combined effect of the carbon flame speed and oxygen ignition delay time.

It is straightforward to find that the ignition delay time is negatively correlated to the O–O reaction rate, which depends on the preheat temperature T_f: $\omega_O(Y_O, T_f) = 5.78 \times 10^{38} \times Y_O^2 \exp(-135.93/T_9^{1/3})$, with the unit of g cm^{-3} s^{-1} and $T_9 = T_f/(10^9$ K) (Fowler et al. 1975). This means when burning a fixed portion of the combustible mixture, a higher preheat temperature leads to a faster reaction rate, and thus a shorter ignition delay time.

Using the carbon flame temperature obtained in the last section, we obtain the ignition delay time of the oxygen burning by Equation (12). As Figures 4(a) and (c) show, with the carbon flame propagating inward, the carbon flame temperature goes up, and the oxygen ignition delay time decreases.

3.3. The Oxygen Spontaneous Propagating Flame Speed

Now, we have obtained the numerical solution of the carbon flame speed u_C and the oxygen ignition delay time τ at different radii; taking them into Equation (4), we thus obtain the spontaneous oxygen flame speed $u_{sp(O)}$. As Figure 4(d) shows, with the flame propagating inward, $u_{sp(O)}$ increases. When propagating to the radius close to one carbon flame thickness, $u_{sp(O)}$ increases to 13.3 times the carbon laminar flame speed. For a C–O white dwarf with density 3.5×10^7 g cm^{-3}, the carbon laminar flame speed u_l is 4.66×10^4 cm s^{-1} (Woosley et al. 2009), so $u_{sp(O)}$ is 6.2 km s^{-1}. This spontaneous oxygen flame speed is much smaller than the sound speed (~ 1500 km s^{-1}), so it cannot form detonation.

For realistic situations, the C–O combustion takes place in turbulent flows, where the flame speed is much larger than the laminar flame speed. In addition to the R-T instability in the laminar flame, there also exist unburned islands formed by vortices in turbulent combustion, the burning of which have a stronger speedup effect on flame propagation. Thus, we consider the flame acceleration in a turbulent flow in the following section.

4. A Spherical Inward-propagating Flame in a Turbulent Flow

For turbulent flows in C–O white dwarfs, there exist many vortices, which range in size from the turbulence large (integral) scale related to the energy injection at ~ 100 km, to the smallest scale of viscous dissipation at $\sim 10^{-3}$ cm. Large-scale vortices wrinkle the flame surface, while small-scale vortices penetrate into the preheat zone of the flame structure, which will increase the flame speed and flame thickness (Denet 1999; Kim & Menon 2000; de Goey et al. 2005). As a consequence, turbulent combustion is divided into different regimes based on the flame thickness/reaction zone thickness and the minimum vortex scale, which can be represented by their respective Karlovitz numbers Ka_f and Ka_r (Law 2010).

4.1. Regimes of Turbulent Combustion in C–O White Dwarfs

Figure 5(a) schematically shows different flame regimes based on the Karlovitz numbers $Ka_f = (\delta_f/\eta)^2$, $Ka_r = (\delta_r/\eta)^2$; where δ_f, δ_r, and η represent the carbon flame thickness, reaction zone thickness and the minimum vortex scale, respectively; note that Ka_f is larger than Ka_r, and the ratio between these two parameters is Ze^2, with the definition of Zel'dovich number being $Ze = \delta_f/\delta_r$. Below the line $Ka_r = Ka_f$, realistic flames in turbulent flows are divided into three regimes and we pay special attention to the line
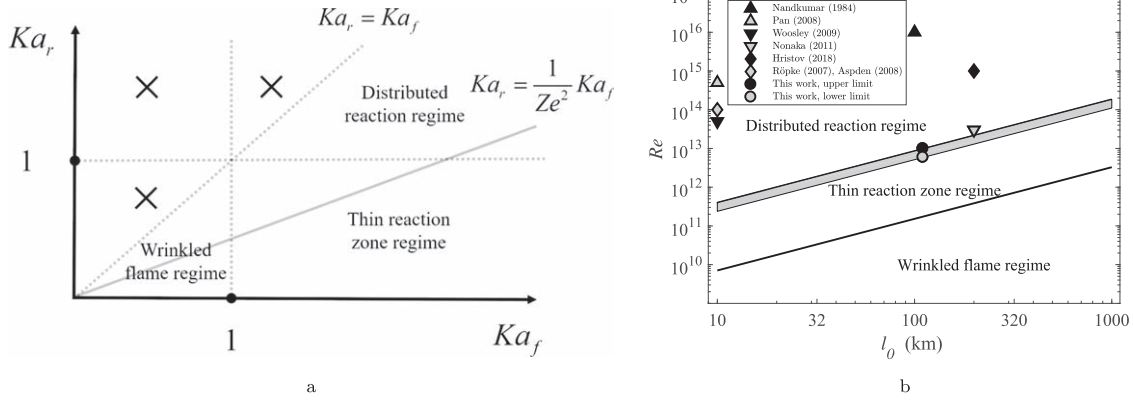
Figure 5. (a) Three turbulent flame regimes in reference to Ka_f and Ka_r. (b) Turbulent regimes in SN Ia in reference to the Reynolds number Re and the integral scale l_0 (Nandkumar & Pethick 1984; Röpke 2007; Aspden et al. 2008; Pan et al. 2008; Woosley et al. 2009; Nonaka et al. 2011; Hristov et al. 2018).

$Ka_r = \frac{1}{Ze^2}Ka_f$, with its slope being $1/Ze^2$. (I) When $Ka_f < 1$, the minimum vortex scale is larger than the flame thickness, and the acceleration of the flame speed is only attributed to the wrinkles of the flame surface. Therefore, this regime is called the wrinkled flame regime. (II) When $Ka_f > 1$ and $Ka_r < 1$, the minimum vortex scale is smaller than the flame thickness but larger than the reaction zone thickness. Thus, a parts of the vortices penetrates the preheat zone of the flame, and the acceleration of the flame speed is attributed to both the wrinkles of the flame surface by large-scale vortices and the strengthening of the thermal and mass diffusions in the preheat zone by small-scale vortices. The flame still has a typical flame structure including a preheat zone and reaction zone; however, the reaction zone is much thinner compared to the strengthened flame thickness. Thus, this regime is called the thin reaction zone regime. (III) When $Ka_r > 1$, the minimum vortex scale is smaller than the reaction zone thickness, so the flame structure is destroyed by such small vortices. A distinct reaction zone does not exist, and the reaction takes place in a much larger distributed space. Thus, this regime is called the distributed reaction regime.

Figure 5(b) shows the turbulent regimes in reference to the Reynolds number Re and turbulence integral scale l_0 in SN Ia. The scale of the smallest vortices is decided by Re and l_0, $\eta = Re^{-3/4}l_0$. Depending on the origin of the turbulence, the integral scale has a wide range, from several kilometers to thousands of kilometers. This is also true for the Reynolds number, which varies in flows with different turbulence strengths. We also mark the turbulent conditions that other authors have studied before in Figure 5(b). Most of them are in the distributed reaction regime, as it is mostly believed that more intense turbulence will more likely lead to DDT. The condition in Nonaka et al. (2011) is close to the thin reaction zone regime, where they conducted a full-star simulation, without resolving the flame structure. For very strong turbulence (large Reynolds number), the distributed reaction regime can be further subdivided based upon the turbulence Damköhler number, $Da_T = \frac{\tau_T}{\tau_n}$, where τ_T is the turbulence timescale and τ_n is the nuclear reaction timescale. Specifically, $Da_T < 1$ is referred to as the well-stirred reactor regime and $Da_T > 1$ is the stirred flame regime (Woosley et al. 2009; Aspden et al. 2010).

4.2. Local Detonations Formed in the Thin Reaction Zone Regime

We next focus on the thin reaction zone regime, where the turbulent flame speed and flame thickness can be measured by the turbulent heat diffusion coefficient, in reference to the laminar flame value as given in the hypothesis of Damköhler (1947): $u_t/u_f = \delta_t/\delta_f = \sqrt{\alpha_t/\alpha_f}$. Here we assume that turbulence has the same strengthening effect on heat and momentum transfer in the preheat zone, so $\alpha_t/\alpha_f = \nu_t/\nu_f$, where u, δ, α, ν represent the flame speed, flame thickness, heat diffusion coefficient, and viscous coefficient; and the subscripts t and f correspond to turbulent and laminar flames, respectively. The boundary of the thin reaction zone regime and the distributed reaction regime is where the minimum scale of the vortices is as large as the thickness of the reaction zone, i.e., $\delta_r = \eta$; thus, $Ka_f = Ze^2$. As the Karlovitz number can be expressed as $Ka_f = \sqrt{\nu_t/\nu_f}$ (Damköhler 1947; Zimont 1979), we have $u_t/u_f = \delta_t/\delta_f = Ze^2$. At this upper boundary of the thin reaction zone regime, the typical Reynolds number is 1.0×10^{13} at the characteristic integral scale $l_0 = 110$ km; correspondingly, the smallest vortex is $\eta = Re^{-3/4}l_0 = 0.002$ cm. For a white dwarf with density 3.5×10^7 g cm^{-3}, the laminar flame speed u_l is 4.66×10^4 cm s^{-1}, flame thickness $\delta_f = 0.041$ cm, and $Ze = 19.0$; then the reaction zone thickness $\delta_r = \delta_f/Ze = 0.0022$ cm, which is roughly as large as the smallest vortices. The above white dwarf condition with a turbulence integral scale of 110 km and Reynolds number 1.0×10^{13} is then denoted as case(A), which has an effective turbulent flame speed of $u_t = 168$ km s^{-1}, and an effective flame thickness $\delta_t = 14.8$ cm (Woosley et al. 2009).

For case (A), the carbon flame temperature is 3.7×10^9 K, and the oxygen ignition delay time τ is about 0.5×10^{-3} s, leading to the distance between the carbon and oxygen flame front being $\Delta X = u_l \times \tau = 23.3$ cm, which is always larger than both the laminar flame thickness δ_f and the strengthened turbulent flame thickness δ_t. Thus, the carbon and oxygen flames keep the distinct two-step flame structure, as shown in Figure 2 even in a turbulent flow. On the other hand, the definition of the oxygen ignition delay time is based on the change of the oxygen mass fraction, which can be measured by the ratio δ_f/u_l in a laminar flame, or equivalently δ_t/u_t in the thin reaction zone regime of a turbulent flame. As a consequence, the contribution of the two parts $1/u_c$ and $d\tau/$
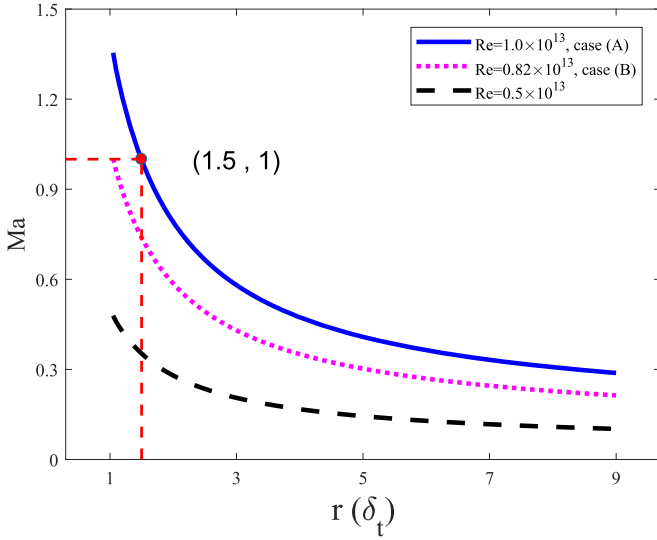
Figure 6. Mach number of the spontaneous oxygen flame speed in turbulent flow. Case (A) represents the upper limit (black filled circle) to keep the thin reaction zone regime with $Re = 1.0 \times 10^{13}$ and $l_0 = 110$ km in Figure 5(b), where the reaction zone thickness is roughly as large as the smallest vortices. Case (B) represents the lower limit (gray filled circle) with $Re = 0.82 \times 10^{13}$ and $l_0 = 110$ km in Figure 5(b), where the oxygen flame speed can reach the sound speed just at the radius of one flame thickness. Between case (A) and (B) the acceleration mechanism discussed here produces a supersonic island flame.

dr in Equation (4) keeps the original portion in the turbulent flow as in laminar flow. So here we adopt the flame acceleration mechanism studied in Section 3 to the thin reaction zone regime in turbulent flame, by simply replacing the laminar flame speed therein with the effective turbulent flame speed.

We then explore the turbulence conditions with $l_0 = 110$ km at different intensities, i.e., with different Reynolds number Re. As shown in Figure 6, for case (A), when the flame propagates to a radius that is 1.5 times the carbon flame thickness (i.e., at $r = 22.2$ cm), the flame speed is equal to the local sound speed of 1627 km s^{-1}, followed by supersonic propagation. For a stronger turbulence, the minimum vortex scale is smaller than the reaction zone thickness. The flame structure will then be destroyed and the above acceleration mechanism for spherical flame fails. Actually, case (A) with $Re = 1.0 \times 10^{13}$ is the upper limit to keep the flame structure in the thin reaction zone regime, denoted as the solid circle in Figure 5(b). When the turbulence becomes weaker, the mixing effect of the small-scale vortices in the flame preheat zone is weakened, and the oxygen flame needs to propagate to a smaller radius to reach the sound speed. Our calculations show that $Re = 0.82 \times 10^{13}$ is the lower limit (denoted as the hollow circle in Figure 5(b) and the dotted line in Figure 6), below which the flame is always subsonic before the flame radius reaches one carbon flame thickness; we denote this turbulence situation as case (B). So for a turbulent flow with $l_0 = 110$ km, the island flame speed can be supersonic only when the turbulence intensity is between case (A) and case (B). Considering turbulent flow at all integral scales, only for the turbulent regime located in the gray narrow band in Figure 5(b) can there be a local supersonic propagating flame when burning the islands. At the turbulent integral scale of $l_0 = 110$ km, previous studies have focused on very strong turbulence with the Reynolds number being larger than 10^{13}. However, the weaker turbulence regime with $0.82 \times 10^{13} < Re < 1.0 \times 10^{13}$ considered here is more
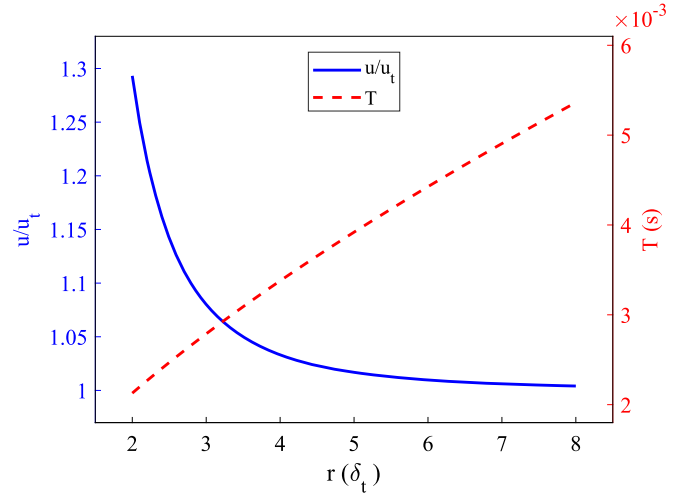

Figure 7. Main flame acceleration effect of a shock wave generated by the burning of a single island with different sizes in units of flame turbulent speed (solid blue curve), and the generation period of islands with different sizes in units of milliseconds (dashed red curve).

likely to occur in SN Ia, as a smaller turbulence speed is required (Röpke 2007; Woosley et al. 2009).

5. Main Flame Acceleration by Shock Waves from the Burning of Islands

For the C–O white dwarf in the turbulence status case (A), when the flame propagates to the radius that is equal to one carbon flame thickness, the Mach number of the spontaneous oxygen flame speed approaches 1.4. Hereafter the flame structure is destroyed and a shock wave forms, with the ratio of the temperature at the two sides of the shock wave being $T_2/T_1 = 1.22$.[5] This means that within one carbon flame thickness to the island center, the temperature reaches 1.22 times the usual flame temperature after the shock heating. Considering further evolution of the shock wave, we assume that it reflects after propagating into the center of the spherical island; so the energy in the sphere with the radius of one flame thickness is uniformly spread to the sphere that is swept by the outward-propagating shock wave. After the shock wave propagates outwardly to the main flame surface located at the boundary of the initially unburned island, the temperature ratio of the shock-heated region to the main flame front is $\lambda_T = (T_2/T_1 - 1)/R_i^3 + 1$, where R_i is the radius of the island. As the speed of the main flame is proportional to the square root of the reaction rate $u \propto \sqrt{\omega_C(T)}$, with $\omega_C(T) \propto \exp(-84.165/T_9^{1/3})$, we can obtain the acceleration of the main carbon flame when a single shock wave heats the main flame: $u/u_t = \exp[42.083/T_9^{1/3} \cdot (1 - \lambda_T^{-1/3})]$ with $T_9 = 3.7$.

After the burning out of one unburned island (and its heating and accelerating to the main flame), another island will form. As a result, the shock waves generated by islands of different sizes heat and speed up the main flame almost continuously. Figure 7 shows both the acceleration effect u/u_t of single shock waves generated by one island (of different sizes), and the generation period $T_i = R_i/u_i$ of one island at this scale (here u_i is the turbulent speed at the island scale R_i). As an example, for

---

[5] The temperature ratio across the flame front is calculated by the shock wave heating as $T_2/T_1 = [2\gamma\ Ma^2 - (\gamma - 1)][(\gamma - 1)Ma^2 + 2]/[(\gamma + 1)^2 Ma^2]$ with $\gamma = 1.33$ the specific heat ratio (Landau & Lifshitz 1959).

Shu, Gao, & Law

islands with a radius 5.5 times the carbon flame thickness, i.e., $R_i = 0.81$ m, which is of the same order of the simulation result in Bell et al. (2004), the speed of the main flame can be accelerated by 1.3% after a single shock wave heating. On the other hand, by adopting the typical viscosity of $\nu = 2 \times 10^6 \, \text{g cm}^{-1} \, \text{s}^{-1}$ (Woosley et al. 2009) to estimate the turbulence speed, the generation period for islands of this size is estimated as 4×10^{-3} s, causing the main flame speed to increase to twice its initial value in about ~ 0.2 s. Although the generation of unburned islands is not necessarily periodic in realistic flames, the above calculations based on the periodic assumption still serve as a good estimation of the main flame heating and speedup.

The main flame accelerating to twice its original flame speed at 0.2 s means that only 1 second is needed to speed up the main flame to $2^5 = 32$ times it origin speed. Given an original subsonic flame speed, e.g., 0.1 Mach number, the increase of the flame speed to a Mach number of 3 occurs easily when the flame propagates for a few hundred kilometers. Consequently, this mechanism is very likely to lead the flame to supersonic propagation and then transit to a detonation when any non-uniformity exists at the flame front. For islands with a relatively smaller radius, the acceleration effect is higher and the period of island generation is shorter. So the detonation heating from smaller unburned islands will more likely lead to the formation of an initial point of the main flame detonation.

6. Conclusion and Discussion

In this paper we study the burning of unreacted islands embedded in the main flame front by analyzing the spherical inward-propagating two-step C–O flame at the flame structure level. By considering the stretch effect on the leading carbon flame, we determined the spontaneous oxygen flame speed (4), which is affected by both the carbon flame speed and the oxygen ignition delay time. We determine such an acceleration mechanism in the unburned islands formed by the R-T instability in a laminar flow using the laminar flame speed, and by R-T islands and vortices in the turbulent flow based on the thin reaction zone regime turbulent flame speed. As the laminar flame speed is small, although the flame speed can be amplified to ~ 10 times, the final speed is always subsonic.

In turbulent flows, for a sub-regime within the thin reaction zone regime (the gray band shown in Figure 5(b)), the oxygen flame can be accelerated to supersonic and generates a shock wave. Specifically, for the C–O white dwarf with density $3.5 \times 10^7 \, \text{g cm}^{-3}$, when the Reynolds number is 1.0×10^{13}, the turbulent integral scale being 110 km (case (A) in this paper, and also the upper boundary of the thin reaction zone regime), the oxygen flame accelerates to supersonic when it propagates inward to $r = 22.2$ cm, which is 1.5 times the turbulent flame thickness. Note that the boundaries of the thin reaction zone regime are determined by comparisons between the characteristic turbulence and flame scales. If additional

effects, e.g., thermal expansion across the flame front, are considered, the boundaries of the regime where the acceleration mechanism apply could vary.

Considering the outward propagation of the reflected shock wave formed in the supersonic burning of the island, the main flame can be heated and sped up. Because the unburned islands continuously form by turbulence vortices over short time intervals, the main flame can be repetitively accelerated by such shock waves, and as a consequence may constitute an initiation mechanism for the main flame detonation.

References

Aspden, A. J., Bell, J. B., Day, M. S., Woosley, S. E., & Zingale, M. 2008, ApJ, 689, 1173
Aspden, A. J., Bell, J. B., & Woosley, S. E. 2010, ApJ, 710, 1654
Bell, J. B., Day, M. S., Rendleman, C. A., Woosley, S. E., & Zingale, M. 2004, ApJ, 608, 883
Chen, Z., Gou, X., & Ju, Y. 2010, CST, 182, 124
Damköhler, G. 1947, Z. Electrochem. Angew. Phys. Chem., 46, 601, https://ntrs.nasa.gov/search.jsp?R=20050009802
de Goey, L., Plessing, T., Hermanns, R., & Peters, N. 2005, P. Combust. Inst., 30, 859
Denet, B. 1999, PhRvE, 59, 2966
Fowler, W. A., Caughlan, G. R., & Zimmerman, B. A. 1975, ARA&A, 13, 69
Gamezo, V., Khokhlov, A., & Oran, E. 2002, P. Combust. Inst., 29, 2803
Hillebrandt, W., & Niemeyer, J. C. 2000, ARA&A, 38, 191
Höflich, P., Khokhlov, A. M., & Wheeler, J. 1995, ApJ, 444, 831
Hristov, B., Collins, D. C., Hoeflich, P., Weatherford, C. A., & Diamond, T. R. 2018, ApJ, 858, 13
Khokhlov, A. M., Oran, E. S., & Wheeler, J. C. 1997, ApJ, 478, 678
Kim, W. W., & Menon, S. 2000, CST, 160, 119
Landau, L. D., & Lifshitz, E. M. 1959, Fluid Mechanics (New York: Pergamon)
Law, C. K. 2010, Combustion Physics (Cambridge: Cambridge Univ. Press)
Law, C. K. 1989, in Symp. (International) on Combustion 22 (Pittsburgh, PA: Combustion Institute), 1381
Malone, C. M., Nonaka, A., Woosley, S. E., et al. 2014, ApJ, 782, 11
Nandkumar, R., & Pethick, C. J. 1984, MNRAS, 209, 511
Nonaka, A., Aspden, A. J., Zingale, M., et al. 2011, ApJ, 745, 73
Pan, L., Wheeler, J. C., & Scalo, J. 2008, ApJ, 681, 470
Pope, S. B. 2000, Turbulent Flows (New York: Cambridge Univ. Press)
Röpke, F. K. 2007, ApJ, 668, 1103
Schmidt, W., Ciaraldi-Schoolmann, F., Niemeyer, J. C., Röpke, F. K., & Hillebrandt, W. 2010, ApJ, 710, 1683
Taylor, G. 1950, RSPSA, 201, 192
Williams, F. A. 1985, Combustion Theory: The Theory of Chemically Reacting Flow Systems (New York: Benjamin-Cummings)
Williams, F. A. 2000, PrECS, 26, 657
Woosley, S. E., Kerstein, A. R., & Aspden, A. J. 2011, ApJ, 734, 37
Woosley, S. E., Kerstein, A. R., Sankaran, V., Aspden, A. J., & Röpke, F. K. 2009, ApJ, 704, 255
Zel'Dovich, Y. 1980, CoFl, 39, 211
Zel'Dovich, Y., Librovich, V., Makhviladze, G., & Sivashinskil, G. 1970, JAMTP, 11, 264
Zimont, V. L. 1979, Combust. Explo. Shock+, 15, 305